**Supporting Information for**

# Proton Transfer Dynamics in the Aprotic Proton Accepting Solvent 1-Methylimidazole

Joseph E. Thomaz,[1,†] Alice R. Walker,[1,2,†] Stephen J. Van Wyck,[1] Jan Meisner,[1,2]
Todd J. Martinez[1,2] and Michael D. Fayer[1,2,*]

[1] Department of Chemistry, Stanford University, Stanford, CA 94305
[2] SLAC National Accelerator Laboratory, Menlo Park, CA 94025
[†] J.E. Thomaz and A.R. Walker contributed equally to this work
Phone: 650 723-4446; E-mail: *fayer@stanford.edu

**Table of Contents**

1. Classical MD Trajectory

2. Clustering Methods

3. Initial QM/MM Results

4. QM/MM AIMD

5. QM Critical Points

Pages 17

Figures 13

Tables 1

This supplemental information is divided into sections for the classical MD, initial QM/MM, QM/MM AIMD, and QM critical point minimizations. The classical MD section includes the dihedral angle over time (Figure S1), solvent exchange of MeIm over time (Figure S2), and cluster analysis of the trajectory snapshots according to various parameters. The initial QM/MM section contains the overall absorption spectrum from classical MD snapshots decomposed by axial and equatorial geometries (Figure S4), and benchmarking for the ω parameter used for the ωPBE TDDFT functional (Figure S5). The QM/MM AIMD section has a representative plot of MeIm distance from the HPTS hydroxyl group over time (Figure S6), the excitation energy of various initial conditions over time (Figures S7-8), and histogrammed excitation energy in two 500fs windows for initial conditions first minimized on $S_0$ (Figure S9). The QM critical point section contains natural orbitals for each critical point with occupation number (Figure S10), the geometric differences between $S_0$ and $S_1$ for axial ($A_I$) and equatorial ($A_{II}$) geometries (Figure S11), and the geometries of the computed NEB transition state approximations (Figure S12).

## 1. Classical MD Trajectory

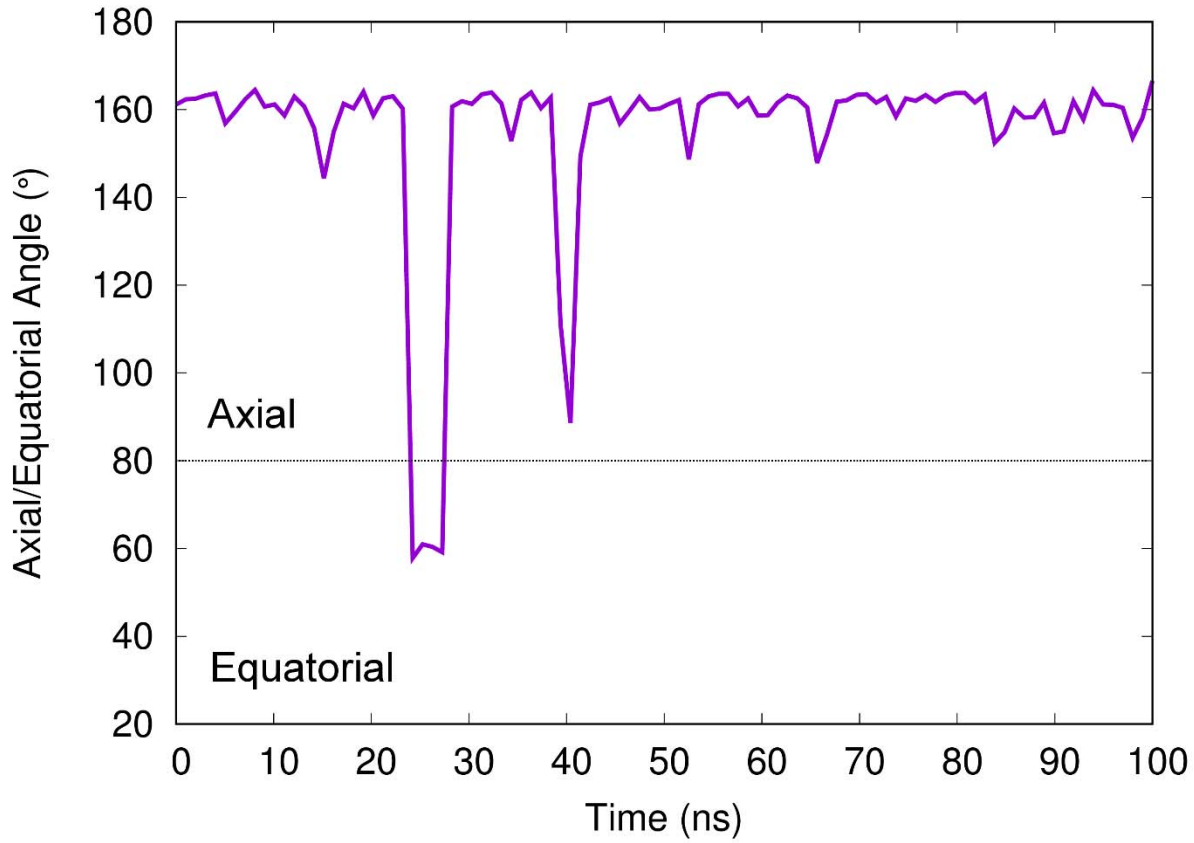


**Figure S1**. HPTS C-O-H angle, which is sensitive to the difference between axial (above 80°) and equatorial (below 80°), is plotted over time for the classical molecular dynamics trajectory. Transitions between axial and equatorial are observed rarely (twice in 100ns) and the dominant configuration is axial.

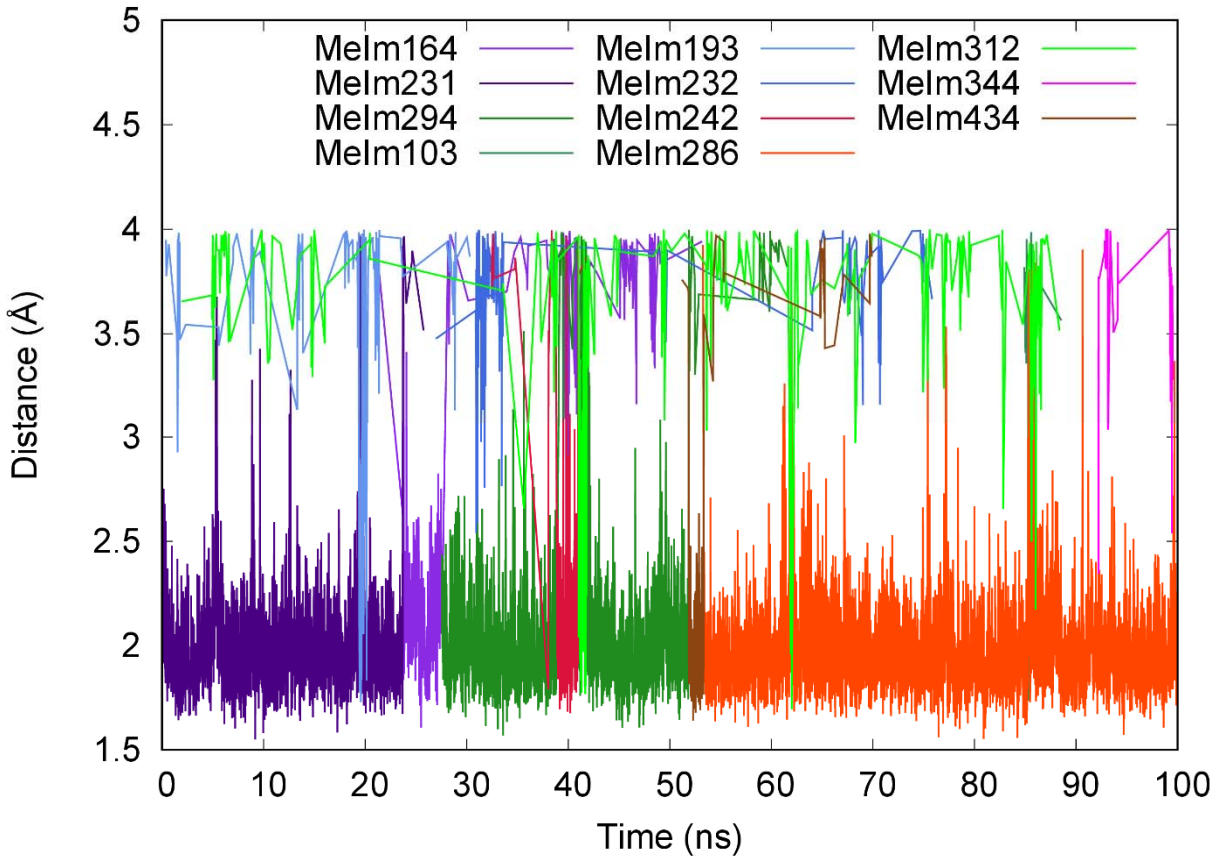


**Figure S2**. Plot of each methylimidazole (MeIm) that hydrogen bonds to HPTS over the course of the 100 ns trajectory. Above 4Å a particular MeIm is considered to be fully dissociated and is not plotted. MeIms are labeled by Amber residue index from the prmtop.

## 2. Clustering Methods

Clustering was performed using Amber's cpptraj program. Structures were clustered according to the radial distribution function (rdf) of the first solvation shell, hydrogen bond distance and dihedral angle of the HPTS hydroxyl group, and by RMSD of the heavy atoms using the 'cluster' keyword. Structures were extracted from the centroid of each cluster. For larger clusters, we included additional structures close to the centroid. In total, 6000 structures were extracted for further analysis with QM/MM.

Figure S3 shows the excitation energy plotted against the different clusters, with points colored by oscillator strength. In each case, they do not show strong correlation with average excitation energy or oscillator strength, aside from a small trend for higher energy excitations to have a lower oscillator strength.

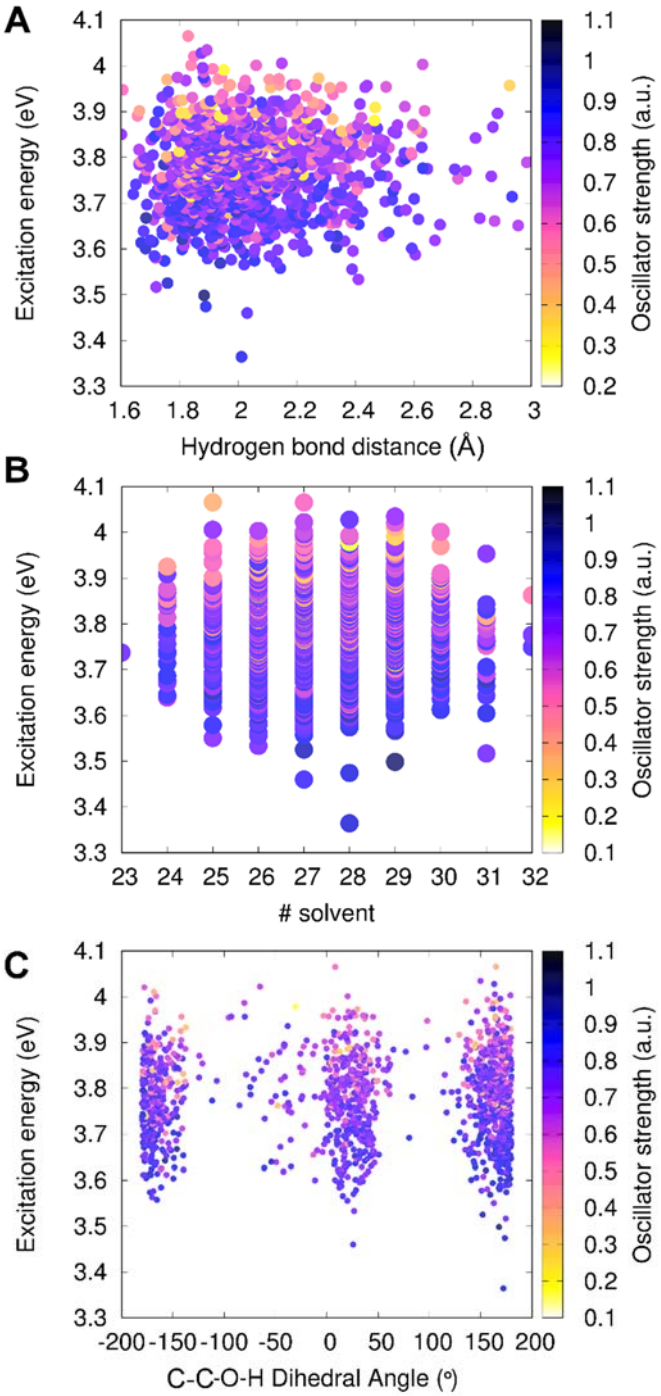


**Figure S3**. Classical MD snapshots were clustered according to various metrics, including hydrogen bond strength in panel A, number of solvent molecules around HPTS in the first solvation shell in panel B, and the dihedral C-C-O-H angle of HPTS in panel C.

## 3. Initial QM/MM Results

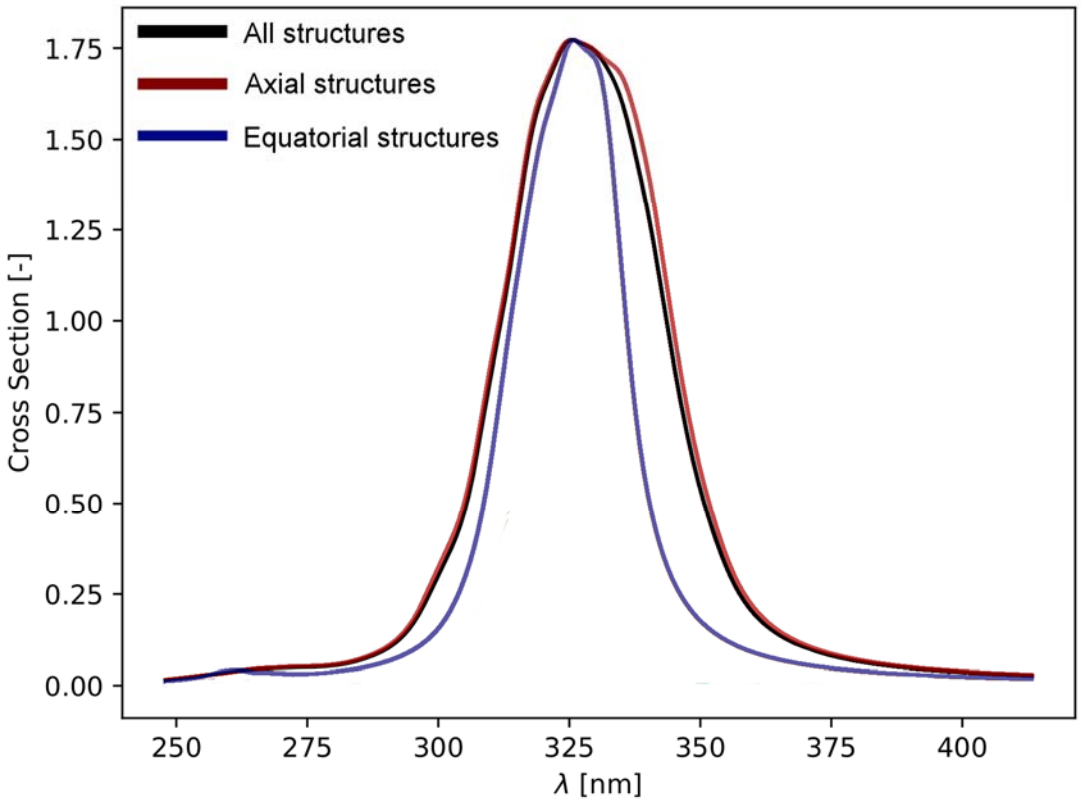


**Figure S4**. Absorption spectra computed with QM/MM (wPBE, 6-31G**) from clustered snapshots from the classical MD trajectory. The net spectrum is shown in black. The spectrum computed from axial snapshots is shown in red, and the spectrum computed from equatorial snapshots is shown in blue. The axial structures have a broader and slightly red-shifted distribution on average compared to the equatorial, but they are not easily differentiable within the peak.

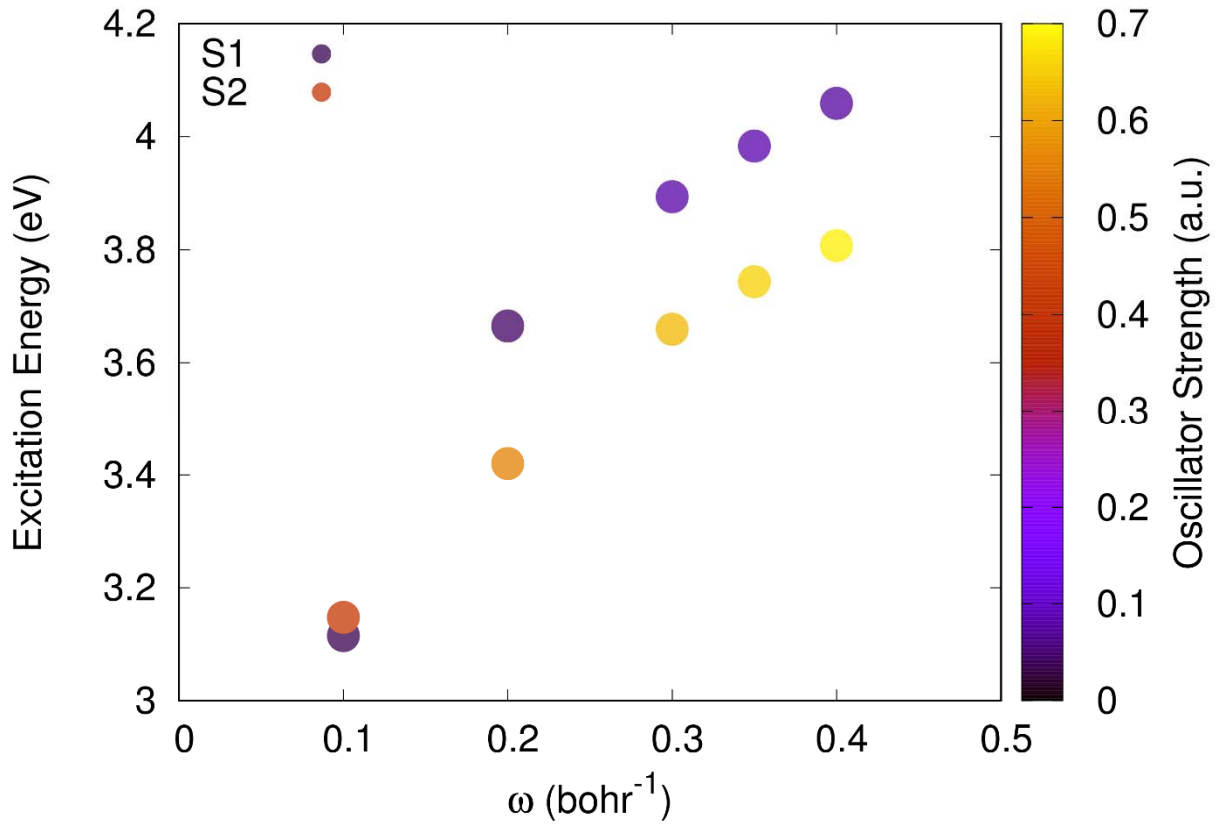


**Figure S5**. A representative set of ω parameter testing for the ωPBE functional. Below 0.2, a spurious low-oscillator strength state can appear involving sodium excitation as $S_1$, which is undesirable for our system.

## 4. QM/MM AIMD

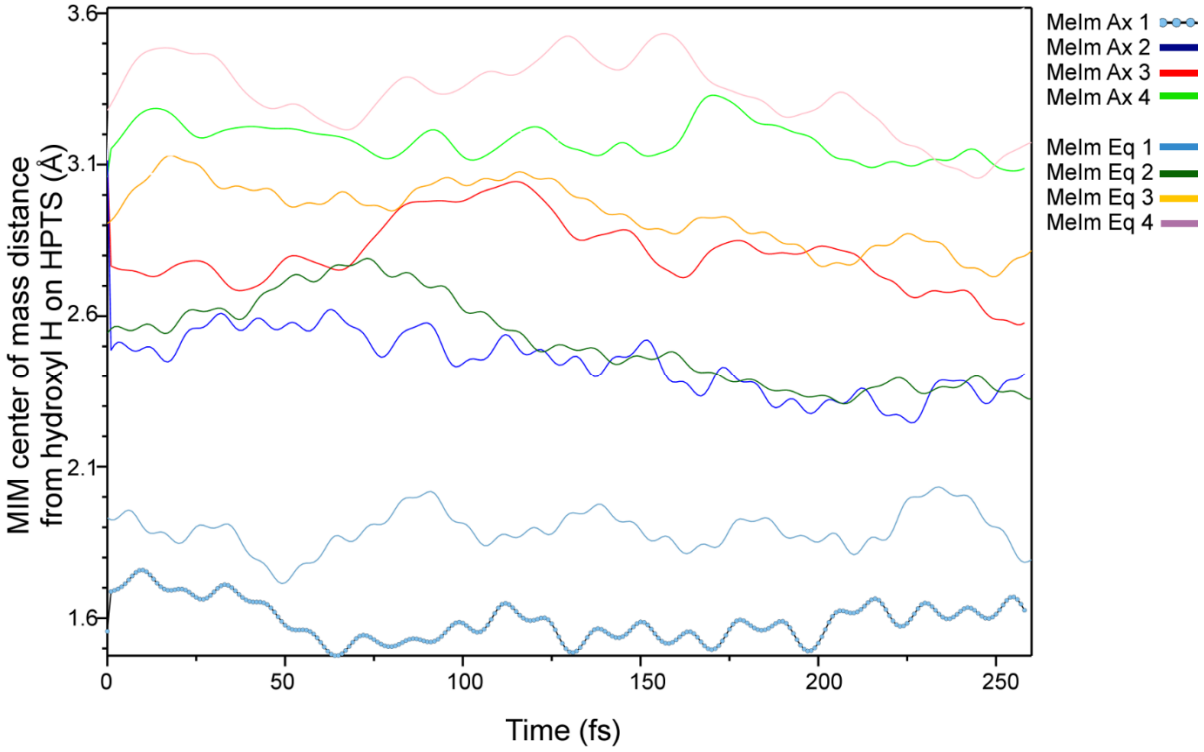


**Figure S6**. Plot of methylimidazole (MIM) molecule distances from the HPTS hydroxyl H over time for representative axial and equatorial initial condition QM/MM AIMD trajectories on the $S_1$ surface. MeIms are numbered by distance, where 1 is the closest MeIm and 4 is the furthest. Over the course of 250 fs, the solvent between from 2.5-2.8 Å (MeIm Ax/Eq 2-3) rearrange the most and show a definite trend of moving towards the HPTS hydroxyl group. In general, the solvent comes closer (MeIm Ax/Eq 2-4), with the exception of the hydrogen-bound MeIm which remains steady for both axial and equatorial. The solvent rearrangement is consistent over time for each.

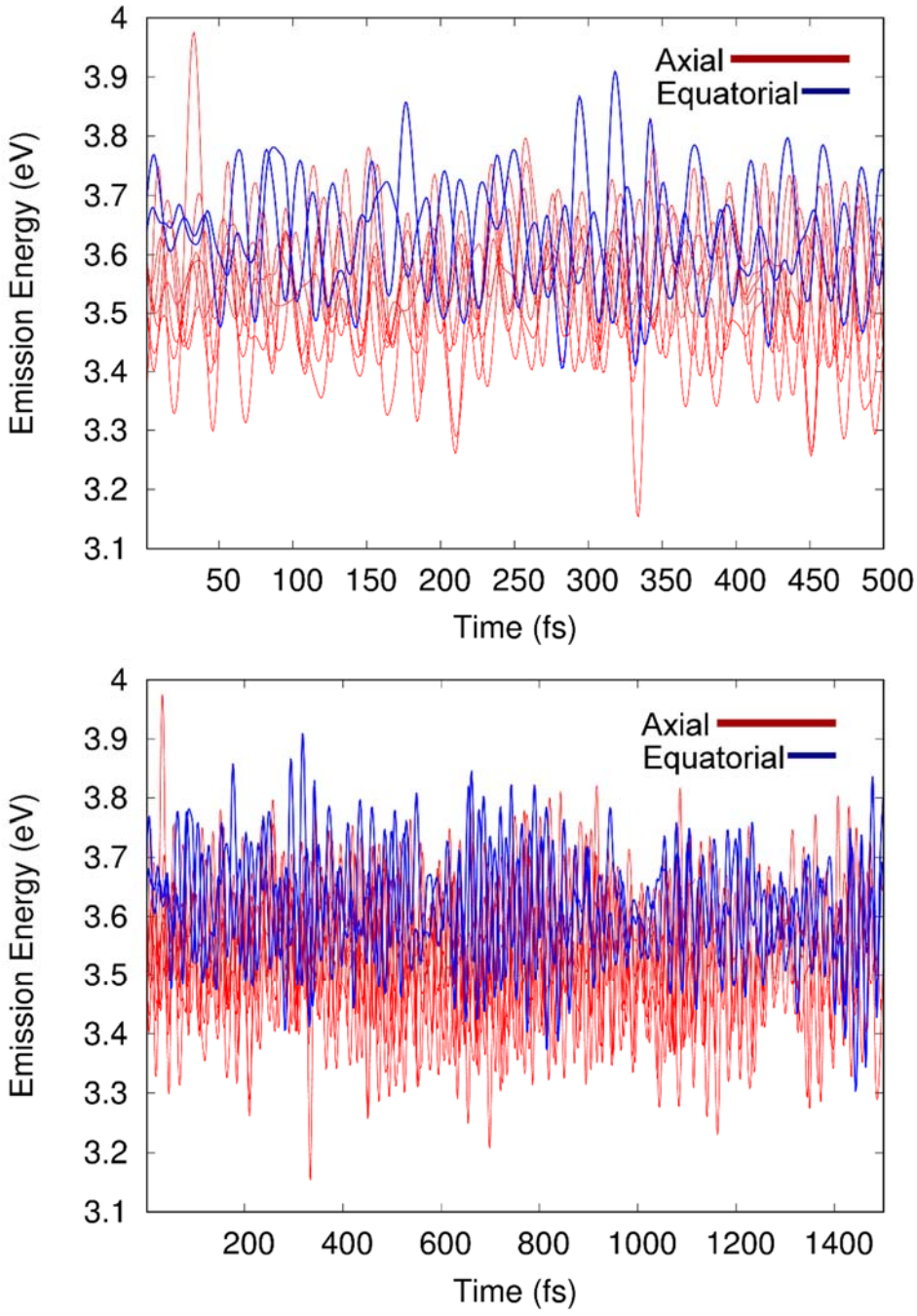


**Figure S7**. Excitation energy computed over time for QMMM/AIMD for various initial conditions from the classical MD, with axial shown in red and equatorial shown in blue. The top shows the first 500 fs of the trajectory, and the bottom shows the trajectory in full.

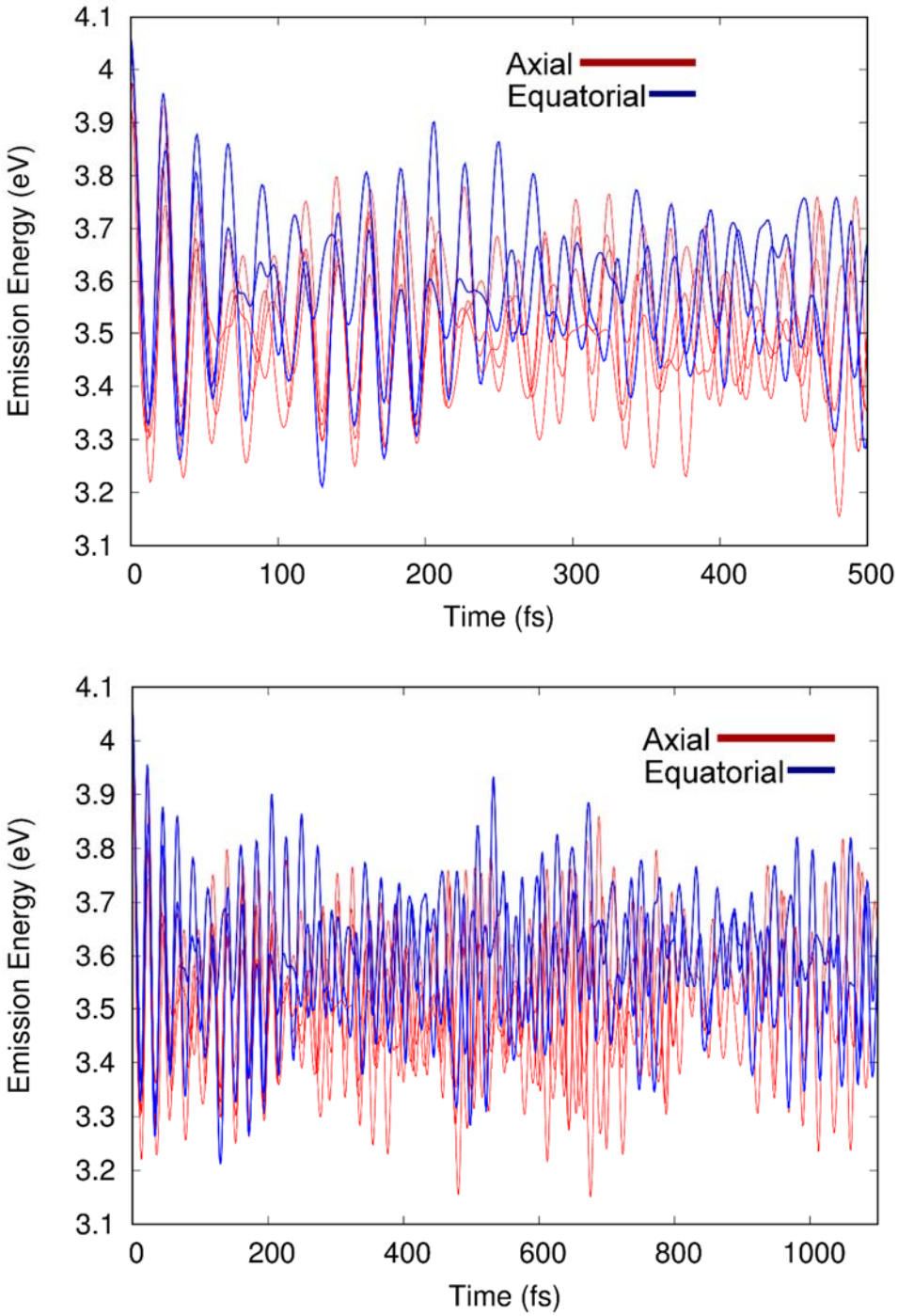


**Figure S8**. Emission energy computed over time for QMMM/AIMD for initial conditions that were first minimized on $S_0$. Axial initial conditions are shown in red, and equatorial are shown in blue. The top shows the first 500 fs of the trajectory, and the bottom shows the trajectory in full.

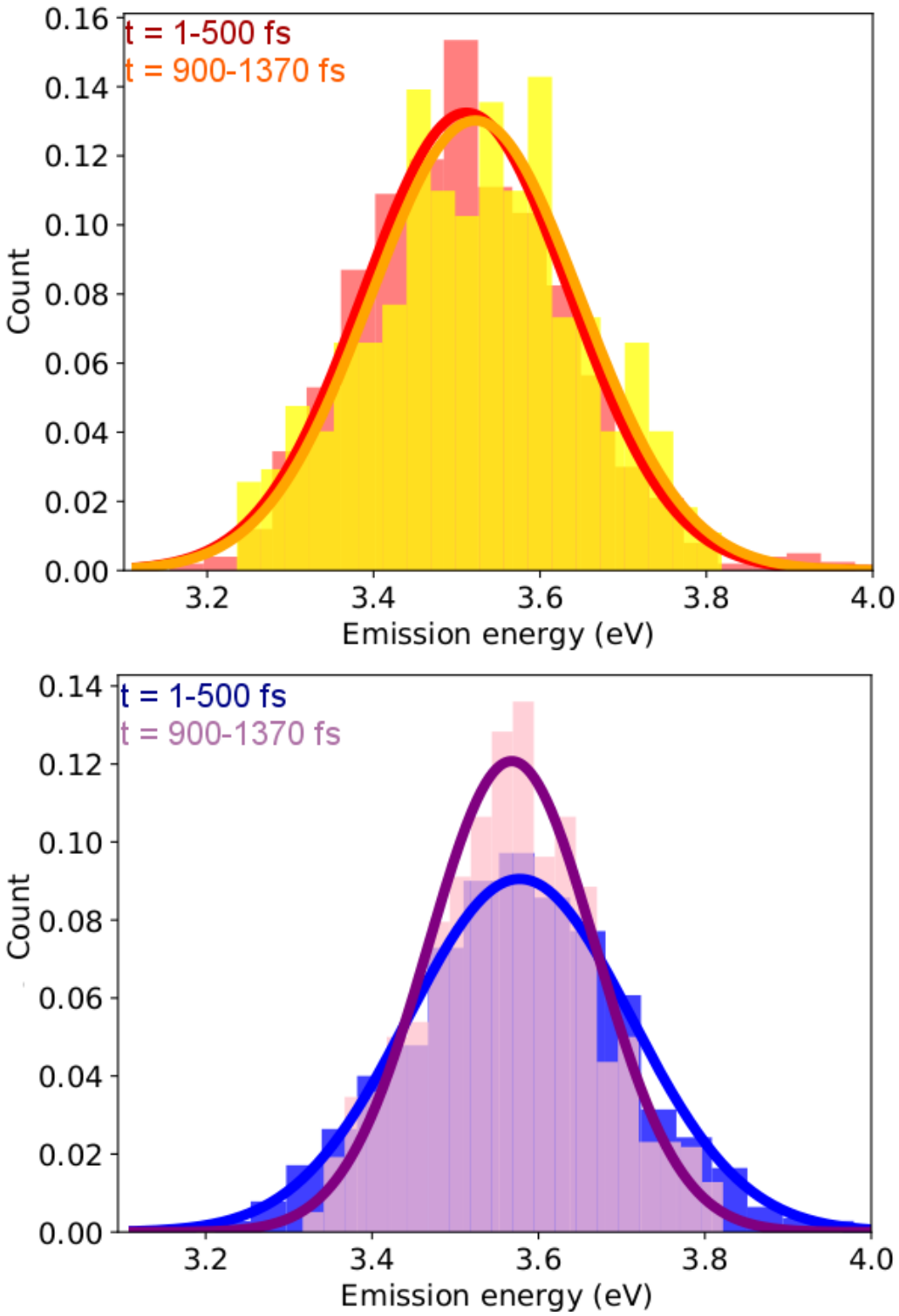


**Figure S9**. Histogram of emission energy in 500 fs time windows for the axial (top) and equatorial (bottom) configurations from the initial conditions that were first minimized on $S_0$. Histograms were computed for 20 bins.

## 5. QM Critical Points

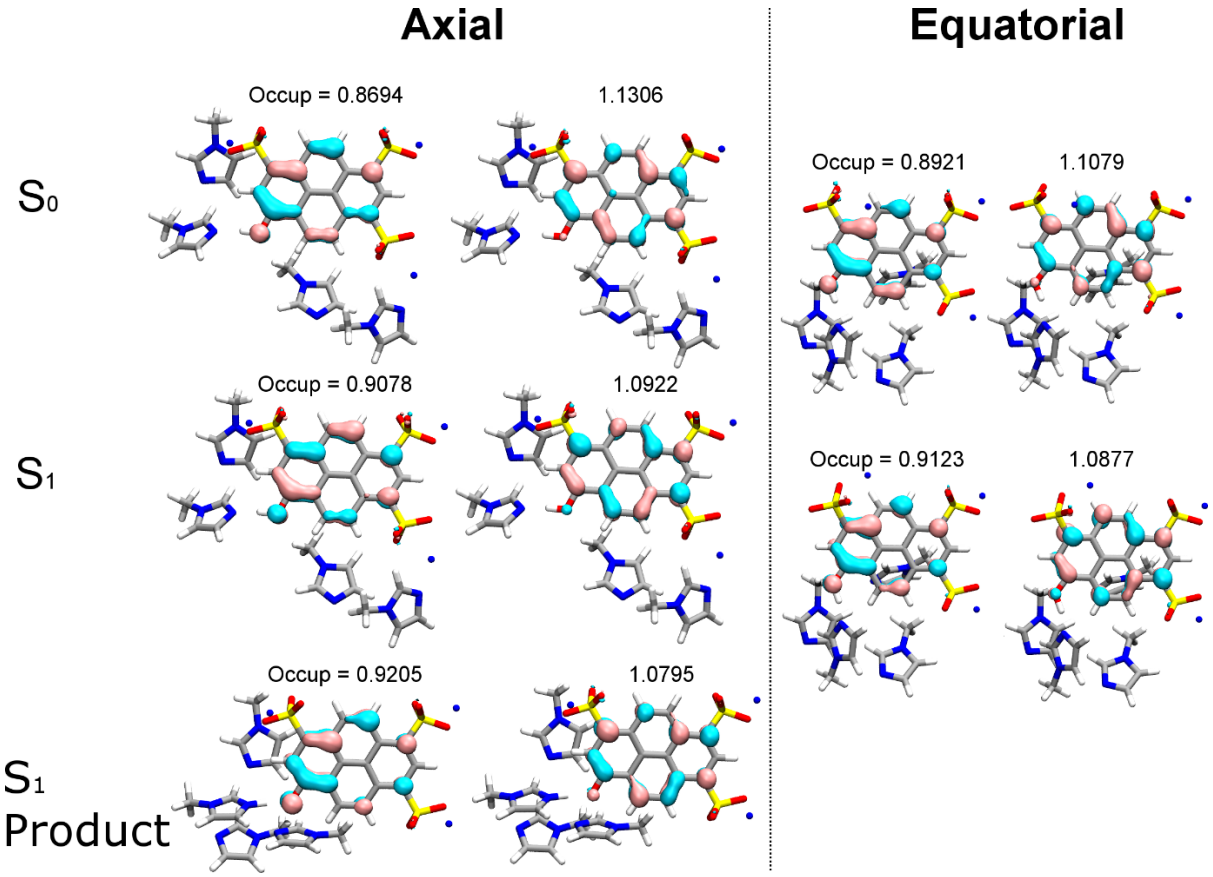


**Figure S10**. Hole/ion pair orbitals for all computed minima in axial and equatorial configurations, shown here with occupation numbers.

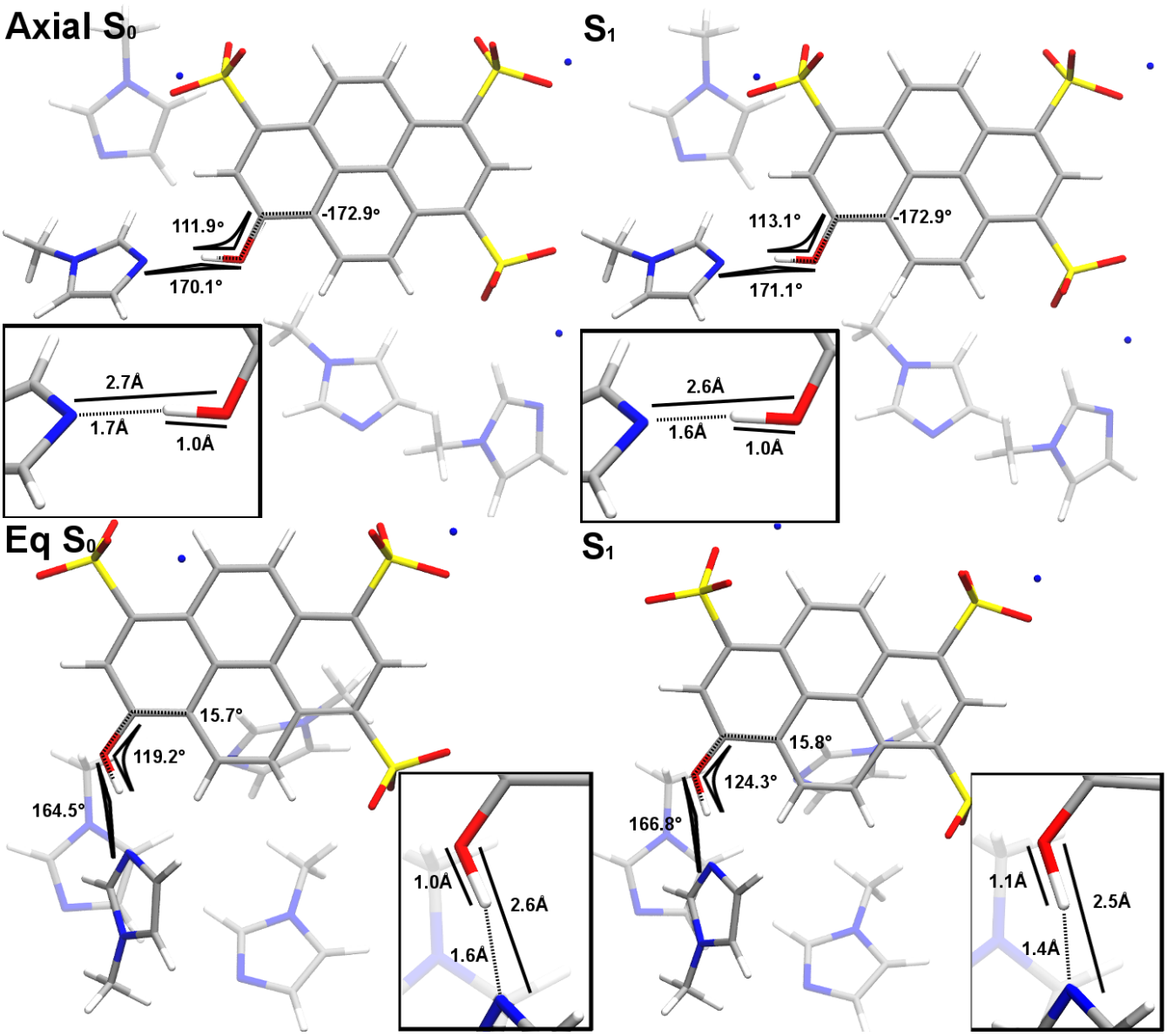


**Figure S11**. Critical point geometries for axial (P) $S_0$ and $S_1$ ($A_I$) on top and equatorial $S_0$ and $S_1$ ($A_{II}$) on bottom. The labeled bonds are O-N, O-H, and H-N, where the N is from the hydrogen bonding MeIm molecule. O-N and H-N are solid black, and H-N is dashed black to denote the hydrogen bond. The labeled angles are $C_2$-O-H and O-H-N, where $C_2$ is the proximal carbon for the hydroxyl group and N is from the hydrogen bonding MeIm molecule. Angles are indicated with black triangles. The labeled dihedral is $C_1$-$C_2$-O-H, where $C_2$ is again the proximal carbon and $C_1$ is one carbon to the right along the long side of the molecule. The dihedral is labeled with a dashed line.

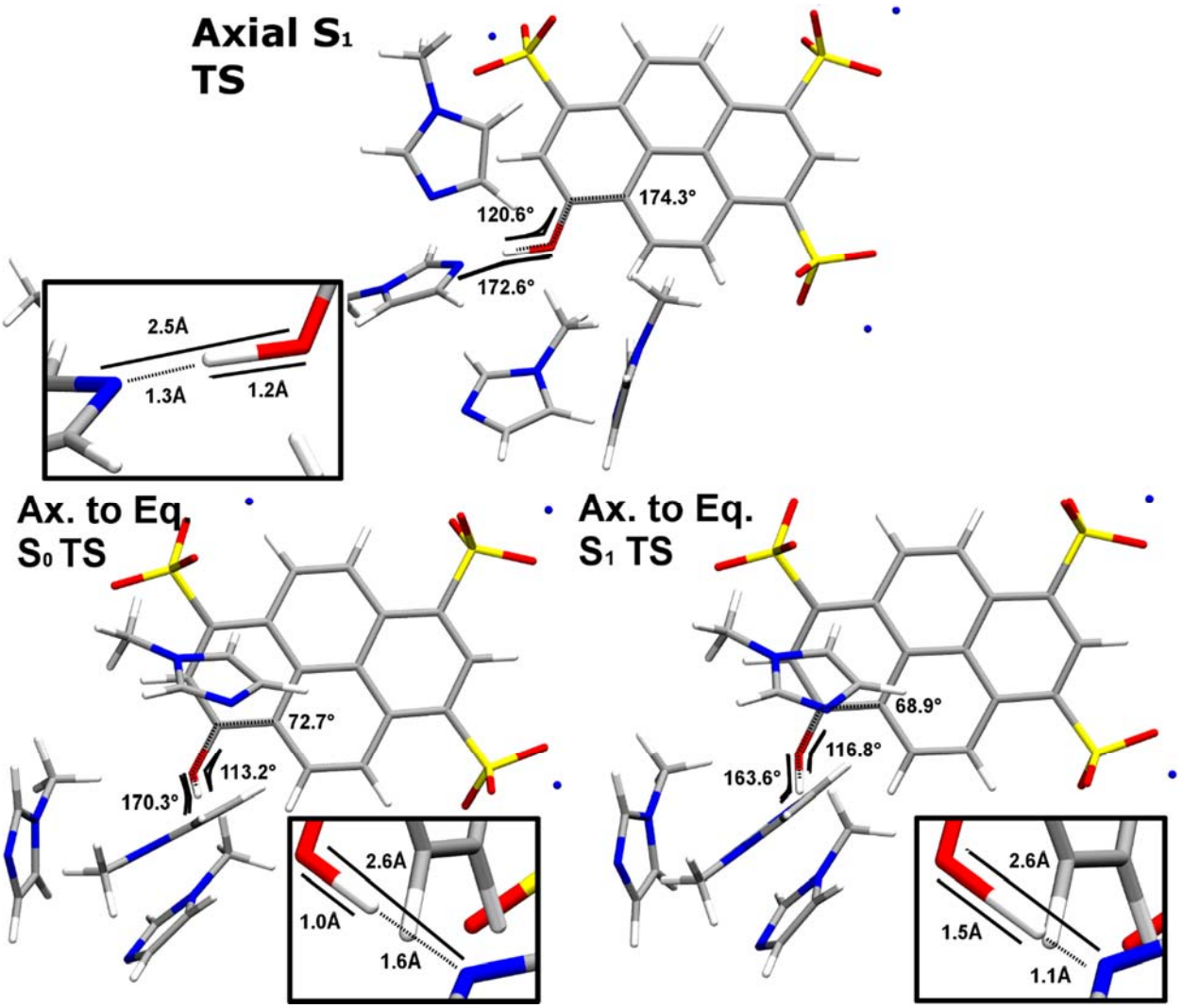


**Figure S12**. Transition state guess geometries from NEB calculations. On top is the transition state guess for the axial $S_1$ deprotonation pathway. On the bottom are the transition state guesses for the axial to equatorial flipping mechanism on $S_0$ (left) and $S_1$ (right). The labeled bonds are O-N, O-H, and H-N, where the N is from the hydrogen bonding MeIm molecule. O-N and H-N are solid black, and H-N is dashed black to denote the hydrogen bond. The labeled angles are $C_2$-O-H and O-H-N, where $C_2$ is the proximal carbon for the hydroxyl group and N is from the hydrogen bonding MeIm molecule. Angles are indicated with black triangles. The labeled dihedral is $C_1$-$C_2$-O-H, where $C_2$ is again the proximal carbon and $C_1$ is one carbon to the right along the long side of the molecule. The dihedral is labeled with a dashed line.

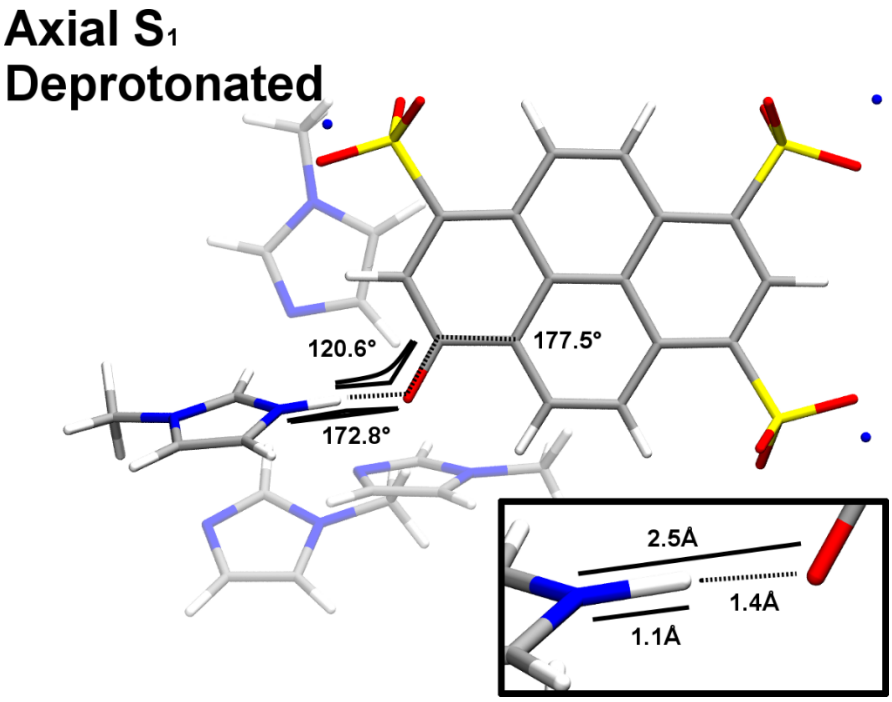


**Figure S13**. Deprotonated S1 product geometry from the axial pathway. The labeled bonds are O-N, O-H, and H-N, where the N is from the newly protonated MeIm molecule. O-N and N-H are solid black, and O-H is dashed to denote the hydrogen bond. The labeled angles are $C_2$-O-H and O-H-N, where $C_2$ is the proximal carbon for the hydroxyl group and N is from the protonated MeIm molecule. Angles are indicated with black triangles. The labeled dihedral is $C_1$-$C_2$-O-H, where $C_2$ is again the proximal carbon and $C_1$ is one carbon to the right along the long side of the molecule. The dihedral is labeled with a dashed line.

**Table S1**. Set of geometry information and energies from Figure 12 in the main text. Shown are the filename for the geometry in the SI, the $S_0$ and $S_1$ energies for each geometry relative to the axial $S_0$ minimum in kcal/mol, and the $S_0$-$S_1$ gap in eV.

| **Geometry** | **SI filename** | **$E_{S0}$ (kcal/mol)** | **$E_{S1}$ (kcal/mol)** | **$\Delta E_{S0/S1}$ (eV)** |
|---|---|---|---|---|
| Axial $S_1$ Deprotonated Minimum | axial_s1_product.xyz | 26.61 | 102.19 | 3.28 |
| Axial ↔ Protonated TS $S_1$ | Ax2Deprot_TS.xyz | 56.39 | 115.97 | 2.58 |
| Axial $S_1$ Minimum | axial_s1.xyz | 4.83 | 85.77 | 3.51 |
| Axial $S_0$ Minimum | axial_s0.xyz | **0.00** | 90.08 | 3.91 |
| Axial ↔ Equatorial TS $S_0$ | Ax2EqS0_TS.xyz | 29.19 | 120.21 | 3.95 |
| Axial ↔ Equatorial TS $S_1$ | Ax2EqS1_TS.xyz | 38.37 | 112.27 | 3.20 |
| Equatorial $S_0$ Minimum | equatorial_s0.xyz | 25.99 | 113.00 | 3.77 |
| Equatorial $S_1$ Minimum | equatorial_s1.xyz | 26.16 | 102.45 | 3.31 |